

Extrapolation and unitarity bounds for the $B \rightarrow \pi$ form factor

I. Sentitemsu Imsong, Alexander Khodjamirian, Thomas Mannel, Danny van Dyk

Theoretische Physik 1, Naturwissenschaftlich-Technische Fakultät, Universität Siegen, D-57068 Siegen, Germany

E-mail: imsong@physik.uni-siegen.de,

khodjamirian@physik.uni-siegen.de, mannel@physik.uni-siege.de,

vandyk@physik.uni-siegen.de

ABSTRACT: We address the problem of extrapolating the vector form factor $f_{B\pi}^+$, which is relevant to $B \rightarrow \pi \ell \nu_\ell$ decays, from the region of small to the region of large momentum transfer. As input, we use the QCD light-cone sum rule at small momentum transfer. We carry out a comprehensive Bayesian uncertainty analysis and obtain correlated uncertainties for the normalization and shape parameters of the form factor. The z -series parametrization for $f_{B\pi}^+$ is employed to extrapolate our results to large momentum transfer, and to compare with the lattice QCD results. To test the validity of our extrapolation we use the upper and lower bounds from the unitarity and positivity of the two-point correlator of heavy-light quark currents. This correlator is updated by including the NNLO perturbative term and the NLO correction to the quark condensate contribution. We demonstrate that an additional input including the form factor, its first and second derivative calculated at one value of momentum transfer from the light-cone sum rules, considerably improves the bounds. This only holds when the correlations between the form factor parameters are taken into account. We further combine our results with the latest experimental measurements of $B \rightarrow \pi \ell \nu_\ell$ by the BaBar and Belle collaborations, and obtain $|V_{ub}| = (3.32_{-0.22}^{+0.26}) \cdot 10^{-3}$ from a Bayesian analysis.

KEYWORDS: Light-Cone Sum Rules, Exclusive Semileptonic B Decays, CKM Matrix Elements

Contents

1	Introduction	1
2	Calculation of the form factor from LCSR and uncertainty analysis	3
3	Extrapolation of the form factor toward large momentum transfer	10
4	Estimation of the strong $B^*B\pi$ coupling	14
5	Unitarity bounds with inputs from LCSR	15
6	Determination of V_{ub} from $\bar{B}^0 \rightarrow \pi^+\ell^-\bar{\nu}$ decays	19
7	Conclusion	22
A	Formulae relevant for the unitarity bounds	23

1 Introduction

Hadronic form factors that are relevant to exclusive semileptonic B decays remain in the center of attention. The $B \rightarrow \pi$ vector form factor $f_{B\pi}^+(q^2)$ in the semileptonic region of the momentum transfer, $0 < q^2 < (m_B - m_\pi)^2$, is indispensable for the determination of the CKM parameter $|V_{ub}|$ from the measurements of $B \rightarrow \pi\ell\nu_\ell$ decay [1–5]. The tension between this determination and the one from inclusive $B \rightarrow X_u\ell\nu_\ell$ decays [6] remains unresolved. On the theory side, the lattice QCD predictions for $B \rightarrow \pi$ form factors are available at large momentum transfer [7–9]. The method of QCD light-cone sum rules (LCSR) provides these form factors at low and intermediate momentum transfer, $q^2 \leq 12 - 15 \text{ GeV}^2$; for the most recent results see [10, 11]. Hence, it is very important to have reliable analytical tools for extrapolating the form factors from the LCSR to the lattice QCD region of q^2 and vice versa. These extrapolations and a reliable assessment of their accuracy are important for both the lattice QCD and the LCSR methods for several reasons: to go beyond the region of their respective applicability; to check their mutual consistence; and to confront the future more accurate results on the shape of the form factors.

For momentum transfer extrapolations, one usually considers a form factor as an analytical (meromorphic) function of the variable q^2 . A conformal mapping from the variable q^2 to the new variable z is applied, so that the complex q^2 plane is mapped onto the unit disc $|z| \leq 1$ in the complex z plane. For $f_{B\pi}^+(q^2)$, the semileptonic region $0 < q^2 < (m_B - m_\pi)^2$ is then transformed to the interval of real and small z , whereas the region of timelike momentum transfer $(m_B + m_\pi)^2 < q^2 < \infty$ is projected onto the unit circle. Owing to the

smallness of z in the semileptonic region, one uses a Taylor expansion for the form factors near $z = 0$, truncating it to a certain maximal order. The most convenient and reliable ansatz commonly used is the BCL version [12] of the z parametrization.

One purpose of this paper is to assess the overall accuracy of this particular parametrization of the form factors. In what follows we will consider only the vector form factor $f_{B\pi}^+(q^2)$ of the $B \rightarrow \pi$ transition for which the available QCD calculations are most accurate to date. A similar analysis of other form factors is deferred to a future work. We will extensively use the LCSR calculations of $B \rightarrow \pi$ form factors carried out in [10, 13] in the $\overline{\text{MS}}$ scheme of the b -quark mass. The earlier results presented in [14] as well as the most recent calculation [11] use the pole-mass scheme and lead to numerically close results.

An important aspect, which so far has been missing in the previous extrapolations of LCSR results from small to large q^2 , is the correlation between the uncertainties of normalization and shape of the form factor. These correlations arise from the simultaneous variations of common input parameters. In earlier analyses uncorrelated uncertainties have been provided that underestimate the accuracy of the LCSR results. To avoid the computation of uncertainty correlations, in [10] the form factor squared was integrated over the LCSR region and then used in the determination of $|V_{ub}|$. However, this procedure leaves aside important aspects of the theory predictions, such as the shape of the form factor that can be compared with anticipated more accurate measurements of the semileptonic differential width. These measurements will provide additional tests for the theoretical calculations. In this paper, we carry out a comprehensive statistical analysis of the form factor uncertainties. From variations of the input parameters in the LCSR we infer theoretical uncertainties of the fitted normalization and shape parameters of the z parametrization, including their correlations.

The second goal of this paper is to control the accuracy of the extrapolation to larger momentum transfer. The widely used z parametrization includes only the first few terms of a Taylor expansion and is therefore model dependent. We suggest to confront the extrapolation with rigorous bounds that follow from the unitarity of the correlation function of heavy-light vector currents, and from the analyticity of the form factors. We update the unitarity bounds for $B \rightarrow \pi$ form factors. Moreover, the bounds obtained using the LCSR inputs at a sufficiently large value of q^2 form a rather narrow band up to $q^2 \simeq 20 \text{ GeV}^2$. These limits become challenging to the extrapolation of the LCSR results and to lattice QCD points.

The plan of the paper is as follows. In section 2 we revisit the $B \rightarrow \pi$ vector form factor as calculated from LCSR, and carry out the statistical analysis of its uncertainties. In section 3 we fit the BCL form of the z parametrization to our LCSR results, and thus provide an extrapolation to large momentum transfers. Based on this extrapolation, we estimate the strong $B^*B\pi$ coupling in section 4. In section 5 we obtain the unitarity bounds from the correlation function, where our LCSR results for the form factor normalization, as well as its first and second derivative with respect to q^2 are used as inputs. The resulting bounds are compared with the extrapolated BCL parametrization. We further use our results in section 6 to determine $|V_{ub}|$ from various experimental results on the exclusive decay $\bar{B}^0 \rightarrow \pi^+ \ell \bar{\nu}_\ell$. Section 7 contains the concluding discussion. For convenience, we

collect necessary elements of the unitarity bounds in the appendix.

2 Calculation of the form factor from LCSR and uncertainty analysis

We use the standard definition of the $B \rightarrow \pi$ form factors

$$\begin{aligned} \langle \pi^+(p) | \bar{u} \gamma_\mu b | \bar{B}(p+q) \rangle \\ = f_{B\pi}^+(q^2) \left[2p_\mu + \left(1 - \frac{m_B^2 - m_\pi^2}{q^2} \right) q_\mu \right] + f_{B\pi}^0(q^2) \frac{m_B^2 - m_\pi^2}{q^2} q_\mu, \end{aligned} \quad (2.1)$$

where, for definiteness, we only consider the transition $\bar{B}^0 \rightarrow \pi^+$. It is our intent to set up the following statistical analysis of the vector form factor $f_{B\pi}^+(q^2)$. The scalar form factor $f_{B\pi}^0(q^2)$, which is of secondary interest, will not be analysed here.

Before turning to the numerical computation, let us shortly outline the derivation of the LCSR. The method was introduced in [15–17] and the first applications to $B \rightarrow \pi$ transitions go back to [18–21]. For a detailed description of the LCSR for the form factor $f_{B\pi}^+(q^2)$ we refer to [13] where all definitions and resulting analytic expressions relevant to our numerical analysis are presented.

One starts from the vacuum-to-pion correlation function of two b -flavoured quark currents:

$$\begin{aligned} i \int d^4x e^{iqx} \langle \pi^+(p) | T \{ \bar{u} \gamma_\mu b(x), m_b \bar{b} i \gamma_5 d(0) \} | 0 \rangle \\ \equiv F((p+q)^2, q^2) p_\mu + \tilde{F}((p+q)^2, q^2) q_\mu, \end{aligned} \quad (2.2)$$

where the invariant amplitude $F((p+q)^2, q^2)$, considered as an analytical function of the variable $(p+q)^2$, is used to access the vector form factor $f_{B\pi}^+(q^2)$ at fixed q^2 . The second amplitude \tilde{F} is only needed for the calculation of the scalar form factor $f_{B\pi}^0(q^2)$.

At $q^2 \ll m_b^2$ and $(p+q)^2 \ll m_b^2$ the intermediate b quark that propagates between the points x and 0 is highly virtual. The T -product of quark currents can therefore be expanded near the light-cone $x^2 \sim 0$. In the resulting operator-product expansion (OPE) the b -quark fields are contracted to a propagator and form perturbatively calculable coefficient functions, whereas the light-quark fields are included in universal vacuum-pion matrix elements of the type $\langle \pi(p) | \bar{u}_\alpha(x) d_\beta(0) | 0 \rangle$ and $\langle \pi(p) | \bar{u}_\alpha(x) G_{\mu\nu}(vx) d_\beta(0) | 0 \rangle$. They absorb nonperturbative effects and are expressed in terms of the pion distribution amplitudes (DAs) with increasing twist. The light-cone OPE yields for the invariant amplitude a generic decomposition:

$$F^{(OPE)}((p+q)^2, q^2) = \sum_{t=2,3,4,\dots} \mathcal{F}^{(t)}((p+q)^2, q^2), \quad (2.3)$$

where each separate twist component

$$\begin{aligned} \mathcal{F}^{(t)}((p+q)^2, q^2) \\ = f_\pi \int \mathcal{D}u \sum_{k=0,1,\dots} \left(\frac{\alpha_s(\mu)}{\pi} \right)^k T_k^{(t)}((p+q)^2, q^2, \{u_i\}, \mu, m_b) \varphi_\pi^{(t)}(\{u_i\}, \mu; \vec{\theta}_{\text{DA}}^{(t)}), \end{aligned} \quad (2.4)$$

factorizes into a perturbatively expandable coefficient function $T_k^{(t)}$ and the pion DAs $\varphi_\pi^{(t)}$ of twist t . The DAs depend on the specific set of input parameters $\vec{\theta}_{DA}^{(t)}$. In the above, μ is the factorization scale and we use the same scale for renormalization of the quark-gluon coupling, b -quark mass and all other running parameters in the adopted $\overline{\text{MS}}$ scheme. The integration variables $\{u_i\} = \{u_1, u_2, \dots\}$ correspond to the fractions of the pion momentum carried by the quark and antiquark in the two-particle Fock state, and the quark, antiquark and gluon in the three-particle Fock state: $\mathcal{D}u \equiv \delta(1 - \sum_i u_i) \prod_i du_i$.

The terms in eq. (2.3) that correspond to higher-twist pion DAs are suppressed by inverse powers of the b -quark virtuality $((p+q)^2 - m_b^2) \sim \bar{\Lambda} m_b$, where $\bar{\Lambda} \gg \Lambda_{QCD}$ does not scale with m_b . This allows for truncation of the OPE. We use the same approximation for the correlation function as in [13], which includes: all LO contributions of the twist 2,3,4 quark-antiquark and quark-antiquark-gluon DA's of the pion; and the NLO, $O(\alpha_s)$ corrections to the twist-2 and twist-3 two-particle coefficient functions. We do not include the recently calculated β_0 estimation for the twist-2 $O(\alpha_s^2)$ contributions [11], since the resulting effect is very small and does not yet represent a complete NNLO calculation. Note that the u, d quark masses and the pion mass are neglected with one exception, the ‘‘chirally enhanced’’ parameter $\mu_\pi \equiv m_\pi^2/(m_u + m_d)$, which appears in the normalization of twist-3 DAs.

The input parameters of the pion DAs, normalized to the pion decay constant f_π , are specified at a fixed normalization scale, typically at $\mu_0 = 1 \text{ GeV}$, with a logarithmic renormalization group evolution to the scale μ . For the twist-2 pion DA these are the coefficients a_n^π of the expansion in terms of Gegenbauer polynomial. We adopt a usual ansatz with two nonvanishing coefficients a_2^π and a_4^π , so that $a_{>4}^\pi = 0$. For the higher twist DAs the conformal expansion is truncated at the first nonleading order (see the analysis in [22]). The pion DAs of nonleading twist are slightly updated with respect to [13]; the definitions we use here can be found in [22] (see also [23]). Beside μ_π , the twist-3 components of the OPE include two further parameters: the normalization of the three-particle DA $f_{3\pi}$ and the coefficient of the nonasymptotic part $\omega_{3\pi}$. Finally we use two additional parameters, δ_π^2 and $\omega_{4\pi}$, for the normalization and nonasymptotic parts of the twist-4 DAs, respectively. To summarize, the set of pion DA parameters is:

$$\begin{aligned}\vec{\theta}_{DA}^{(2)} &= (a_2^\pi, a_4^\pi), \\ \vec{\theta}_{DA}^{(3)} &= (\mu_\pi(2 \text{ GeV}), f_{3\pi}(1 \text{ GeV}), \omega_{3\pi}(1 \text{ GeV})), \\ \vec{\theta}_{DA}^{(4)} &= (\delta_\pi^2(1 \text{ GeV}), \omega_{4\pi}(1 \text{ GeV})).\end{aligned}$$

In order to link the correlation function to the $B \rightarrow \pi$ form factor, we use the hadronic dispersion relation for the invariant amplitude in the variable $(p+q)^2$, but at a fixed value of q^2 ,

$$F((p+q)^2, q^2) = \frac{2m_B^2 f_B f_{B\pi}^+(q^2)}{m_B^2 - (p+q)^2} + \dots \quad (2.5)$$

The form factor enters the ground-state B -meson contribution only as a product with the B -meson decay constant f_B . The remaining sum over excited and continuum hadronic states with quantum numbers of the B -meson, indicated by ellipses in eq. (2.5), is approximated

using (semi-local) quark-hadron duality: the sum in the hadronic dispersion relation is replaced by the quark-gluon spectral density, obtained by calculating $\text{Im } F^{(OPE)}(s, q^2)$ from the OPE eq. (2.3) at $(p+q)^2 \equiv s > m_b^2$. The duality approximation introduces the effective threshold parameter s_0^B . After the Borel transformation $(p+q)^2 \rightarrow M^2 \sim \bar{\Lambda} m_b$, the resulting LCSR for the $B \rightarrow \pi$ form factor has the following form

$$f_{B\pi}^+(q^2; \vec{\theta}) = \left(\frac{e^{m_B^2/M^2}}{2m_B^2 [f_B]_{2\text{ptSR}}} \right) \int_{m_b^2}^{s_0^B} ds \sum_{t=2,3,4} \frac{1}{\pi} \text{Im } \mathcal{F}^{(t)}(s, q^2) e^{-s/M^2}. \quad (2.6)$$

Anticipating the following numerical and statistical analysis, we introduce $\vec{\theta}$, the set of all input parameters on which the r.h.s. of the LCSR depends. The components of $\vec{\theta}$ shall later be varied within certain intervals. Furthermore, the label “2ptSR” at the decay constant f_B in eq. (2.6) indicates that we calculate it from the QCD sum rule for the two-point correlation function of $m_b \bar{b} i \gamma_5 d$ currents. Without going into details, which can be found e.g. in the recent update of this sum rule in [24], we write the result of this calculation schematically as

$$[f_B^2]_{2\text{ptSR}} = \left(\frac{e^{m_B^2/\bar{M}^2}}{m_B^4} \right) \bar{\mathcal{F}}(\bar{M}^2, \bar{s}_0^B, \alpha_s, \mu, m_b, \vec{\theta}_{\text{cond}}). \quad (2.7)$$

Here, the quantity $\bar{\mathcal{F}}$ represents the result of the OPE for the two-point correlation function. It contains perturbative and nonperturbative contributions; the latter involve vacuum condensate densities of growing mass dimension. In this sum rule, owing to the power suppression of the terms with higher-dimensional condensates, only terms up to the mass dimension six are taken into account in the OPE. The corresponding set of input parameters for the vacuum condensates in the adopted approximation,

$$\vec{\theta}_{\text{cond}} = \left(\langle \bar{q}q \rangle (2 \text{ GeV}), \langle \frac{\alpha_s}{\pi} G^2 \rangle, m_0^2, r_{\text{vac}} \right), \quad (2.8)$$

includes the quark-condensate density at the reference scale, the (scale independent) gluon-condensate density, the ratio of quark-gluon to quark-condensate density $m_0^2 \equiv \langle \bar{q}G\bar{q} \rangle / \langle \bar{q}q \rangle$, and the coefficient r_{vac} that parametrizes the factorization in the four-quark condensate density. We neglect a weak scale dependence of the higher-dimensional condensate densities. Note that we use the two-point sum rule to NLO accuracy, to stay consistent with the overall accuracy of the LCSR.

Summarizing the input parameters in eq. (2.6), where eqs. (2.7) and (2.4) are substituted, we have for the set of variable inputs:

$$\vec{\theta} \equiv \left(\alpha_s(M_Z), \bar{m}_b(m_b), \vec{\theta}_{DA}^{(2,3,4)}, \vec{\theta}_{\text{cond}}, M^2, s_0^B, \bar{M}^2, \bar{s}_0^B \right). \quad (2.9)$$

We exclude from this set the meson masses m_B , m_π and the pion decay constant f_π that are all measured with a negligibly small errors. We also exclude the combined renormalization and factorization scale μ . This follows after explicitly checking that variation of μ in the preferred interval [2.5 GeV, 4 GeV], chosen according to [10], yields shifts to the mean

values which are small compared to the remaining parametric uncertainties. Within the perturbative expansion of the invariant amplitudes $F^{(\text{OPE})}$,

$$F^{(\text{OPE})} = \sum_{k=0,1,2,\dots} \left(\frac{\alpha_s C_F}{4\pi} \right)^k F^{(k)}, \quad (2.10)$$

we also investigate the effects of hypothetical NNLO terms $F^{(2)}$. We estimate the latter as

$$|F^{(2)}| \leq \left| \frac{[F^{(1)}]^2}{F^{(0)}} \right|, \quad (2.11)$$

and find the associated uncertainty to be well below 0.05% for $0 \leq q^2 \leq 12 \text{ GeV}^2$.

In addition, the derivatives of the LCSR and of the two-point sum rule with respect to $-1/M^2$ and $-1/\overline{M}^2$, respectively, should reproduce the B -meson mass squared:

$$[m_B^2]_{\text{LCSR}} = \frac{\int_0^{s_0^B} ds s \text{Im} F^{(\text{OPE})}(s, q^2) e^{-s/M^2}}{\int_0^{s_0^B} ds \text{Im} F^{(\text{OPE})}(s, q^2) e^{-s/M^2}}, \quad (2.12)$$

$$[m_B^2]_{\text{2ptSR}} = \frac{d/d(-1/\overline{M}^2) \overline{\mathcal{F}}(\overline{M}^2, \overline{s}_0^B, \dots)}{\overline{\mathcal{F}}(\overline{M}^2, \overline{s}_0^B, \dots)}.$$

We will use these relations later on in our statistical analysis, where we constrain both $[m_B]_{\text{LCSR}}$ and $[m_B]_{\text{2ptSR}}$ to lie within a given small interval around the measured B -meson mass. This is a more general constraint than the one used in the previous analyses of these sum rules, such as in [10, 13]. There, the threshold parameters were adjusted to the B -meson mass by variation of only the Borel parameter.

In table 1 we collect all input parameters and their adopted variation ranges used in our numerical calculation, indicating also their sources. A few comments are in order. Note that we use the strange quark mass determination ¹ from [6] in a combination with the very accurate ChPT relation [25] to determine $m_u + m_d$ that in turn yields the quark-condensate density and the parameter μ_π . The intervals for a_2^π, a_4^π were estimated in [10] by fitting the LCSR for the pion electromagnetic form factor to the experimental data. Our choice of the pion twist-2 DA is consistent with the two-point sum rule estimates of a_2^π . Moreover, as shown in [10] the pion DA with four nonvanishing Gegenbauer moments, based on the updated analysis of the LCSR for the photon-pion transition form factor [27] (see also [28]), produces very similar results for the $B \rightarrow \pi$ form factor. Furthermore, we specify the uniform renormalization and factorization scale μ as well as the Borel-parameter intervals for both LCSR and 2-point sum rule according to the choice in [10] and [24]. The broad ranges for both threshold parameters will be substantially constrained by the B -meson mass relations. In our numerical analysis, we use four-loop running of α_s

¹We double the error to be consistent with the typical accuracy of non-lattice determinations of m_s .

Parameter	value/interval	unit	prior	source/comments
quark-gluon coupling and quark masses				
$\alpha_s(m_Z)$	0.1184 ± 0.0007	—	gaussian @ 68%	[6]
$\bar{m}_b(\bar{m}_b)$	4.18 ± 0.03	GeV	gaussian @ 68%	[6]
m_s	95 ± 10	MeV	—	[6] (error doubled)
$R \equiv 2m_s/(m_u + m_d)$	24.4 ± 1.5	—	—	ChPT, [25]
$m_u + m_d$	7.8 ± 0.9	MeV	gaussian @ 68%	$2m_s/R$
hadron masses				
m_B	5279.58	MeV	—	[6]
m_π	139.57	MeV	—	[6]
vacuum condensate densities				
$\langle \bar{q}q(2\text{GeV}) \rangle$	$-(277_{-10}^{+12})^3$	MeV ³	—	$m_\pi^2 f_\pi^2 / 2(m_u + m_d)$
$\langle \frac{\alpha_s}{\pi} G^2 \rangle$	[0.000, 0.018]	GeV ⁴	uniform @ 100%	[26]
m_0^2	[0.6, 1.0]	GeV ²	uniform @ 100%	[26]
r_{vac}	[0.1, 1.0]	—	uniform @ 100%	[26]
parameters of the pion DAs				
f_π	130.4	MeV	—	[6]
$a_{2\pi}(1\text{GeV})$	[0.09, 0.25]	—	uniform @ 100%	[10]
$a_{4\pi}(1\text{GeV})$	[-0.04, 0.16]	—	uniform @ 100%	[10]
$\mu_\pi(2\text{GeV})$	2.5 ± 0.3	GeV	—	$m_\pi^2 / (m_u + m_d)$
$f_{3\pi}(1\text{GeV})$	[0.003, 0.006]	GeV ²	uniform @ 100%	[22]
$\omega_{3\pi}(1\text{GeV})$	[-2.2, -0.8]	—	uniform @ 100%	[22]
$\delta_\pi^2(1\text{GeV})$	[0.12, 0.24]	GeV ²	uniform @ 100%	[22]
$\omega_{4\pi}(1\text{GeV})$	[0.1, 0.3]	—	uniform @ 100%	[22]
sum rule parameters and scales				
μ	3.0	GeV	—	[10, 24]
M^2	16.0 ± 4.0	GeV ²	gaussian @ 68%	[10]
s_0^B	[30.0, 45.0]	GeV ²	uniform @ 100%	
\bar{M}^2	5.5 ± 1.0	GeV ²	gaussian @ 68%	[24]
\bar{s}_0^B	[29.0, 44.0]	GeV ²	uniform @ 100%	

Table 1. Input parameters used in the numerical analysis. The prior distribution $P_0(\vec{\theta})$ is a product of individual priors, either uniform or gaussian. The uniform priors cover the stated intervals with 100% probability. The gaussian priors cover the stated intervals with 68% probability, and the central value corresponds to the mode of the prior. For practical purposes, variates from the gaussian priors are only drawn from their respective 99% intervals.

and quark masses, whereas for the nonperturbative scale-dependent parameters of the pion DA's one-loop (LL) renormalization suffices.

Important is that there are in fact more correlations between many of the input parameters, apart from the one between the quark-condensate density, μ_π and light-quark masses that is taken into account. For example, the normalization and nonasymptotic coefficients of higher twist pion DAs are themselves obtained from two-point sum rules; i.e., they depend on the condensate parameters. However, the task of including all these “hidden” correlations remains outside the scope of our present work. It demands a global simultaneous numerical analysis of all sum rules involved in the determination of the input parameters. We make here the simplifying assumption that all parameters entering $\vec{\theta}$ are independent and their individual uncertainties are therefore not correlated. Due to this conservative assumption, we expect that the uncertainties estimated in this paper are in fact somewhat larger than the true ones.

We now turn to the details of the statistical analysis. Throughout this work we use a Bayesian approach (see e.g. [29] for a review) to determine the mean values and theoretical uncertainties for the form factor $f_{B\pi}^+(q^2)$. To this end, we have implemented the two-point sum rule for f_B , as well as the LCSR for $f_{B\pi}^+$ within EOS [30], a HEP program for the computation of flavour observables. Throughout this work, all numerical results are obtained using EOS. We start from the region of momentum transfer where the LCSR is applicable. The upper limit of this region is chosen to be $q^2 = 12 \text{ GeV}^2$ as in [10], to guarantee a good convergence of the light-cone OPE. This is reflected by the very small size of the twist-4 contribution to the LCSR. We express our prior knowledge of the input parameters $\vec{\theta}$ through the *prior distribution* $P_0(\vec{\theta})$, for which we use a product of uncorrelated distributions for each element of $\vec{\theta}$. The individual factors are either uniform or gaussian distributions. The uniform distributions cover the intervals listed in table 1 at 100% probability. The gaussian ones use the listed intervals so that the central value is the mode, and the intervals contain 68% of accumulated probability. However, the allowed interval for such parameters is restricted to their respective 99% probability intervals for practical purposes.

We now construct a *likelihood* $P(m_B|\vec{\theta})$ that incorporates *purely theoretical* constraints on our parameter space. Specifically, we demand that theory determinations of the B -meson mass $[m_B]_{\text{LCSR}}(q^2)$ and $[m_B]_{\text{2ptSR}}$ from eq. (2.12) agree with the experimentally measured value within 1% at 68% probability. It should be emphasized that the magnitude of σ_B stems purely from our estimates. We thus use a gaussian distribution for the likelihood with the standard deviation parameter $\sigma_B = m_B \cdot 1\% \simeq 0.053 \text{ GeV}$. The complete likelihood reads

$$P(m_B|\vec{\theta}) = \mathcal{N}(m_B, \sigma_B; [m_B]_{\text{2ptSR}}(\vec{\theta})) \times \mathcal{N}(m_B, \sigma_B; [m_B]_{\text{LCSR}}(\vec{\theta}; q^2 = 0)), \quad (2.13)$$

where $\mathcal{N}(\mu, \sigma; x)$ denotes the probability density function for the gaussian distribution of x around the mean μ with standard deviation σ . From our prior and likelihood follows the *posterior distribution* according to Bayes' theorem,

$$P(\vec{\theta}|m_B) = \frac{P(m_B|\vec{\theta})P_0(\vec{\theta})}{\int d\vec{\theta} P(m_B|\vec{\theta})P_0(\vec{\theta})}. \quad (2.14)$$

We observe that the likelihood has significant impact on the posterior distribution of the threshold parameters s_0^B and \bar{s}_0^B . Their marginalized one-dimensional posteriors resemble a gaussian distribution, with approximate 68% intervals of $(41 \pm 4)\text{GeV}^2$ and $(35 \pm 2)\text{GeV}^2$, respectively. The remainder of the input parameters exhibit virtually no difference between their respective priors and marginalized one-dimensional posteriors. While eq. (2.12) at $q^2 = 0$ perfectly reproduces the experimental B -meson mass, we observe that the mode of the distribution of $[m_B]_{\text{LCSR}}(q^2 = 10 \text{ GeV}^2)$ is shifted with respect to m_B by $\sim 2.5\%$.

In order to obtain the values and uncertainties for the form factor results from our input parameters, we carry out an uncertainty propagation. This is achieved by computing $5 \cdot 10^4$ samples of the joint *posterior predictive distribution* $P(\vec{F}|m_B)$,

$$P(\vec{F}|m_B) = \int d\vec{\theta} \delta(\vec{F} - \vec{F}(\vec{\theta})) P(\vec{\theta}|m_B), \quad (2.15)$$

of our quantities of interest \vec{F} . For the latter we chose the normalization of the form factor as well as its first and second derivative with respect to q^2 . We evaluate these quantities at two points $q^2 = 0$ and $q^2 = 10 \text{ GeV}^2$ located at the opposite ends of the LCSR region:

$$\vec{F} \equiv (f_{B\pi}^+(0), f_{B\pi}^{+'}(0), f_{B\pi}^{+''}(0), f_{B\pi}^+(10 \text{ GeV}^2), f_{B\pi}^{+'}(10 \text{ GeV}^2), f_{B\pi}^{+''}(10 \text{ GeV}^2)). \quad (2.16)$$

In the above, we denote the first and second derivative of $f_{B\pi}^+(q^2)$ with respect to q^2 as $f_{B\pi}^{+'}(q^2)$ and $f_{B\pi}^{+''}(q^2)$, respectively.

We find that the one-dimensional marginal distributions for each element of \vec{F} resemble a gaussian distributions to good accuracy. The one-dimensional marginalised posterior of $f_{B\pi}^{+''}$ is slightly leptokurtic, with $\text{Kurt} \sim 4$. The remainder of the one-dimensional posteriors are approximately mesokurtic, with $|\text{Kurt}| < 0.25$. We feel therefore confident to approximate the true distribution $P(\vec{F}|m_B)$ through a six-dimensional multivariate gaussian distributions, $P(\vec{F}|m_B) \simeq \mathcal{N}_6(\vec{\mu}^F, \Sigma^F; \vec{F})$. We obtain the mean vector $\vec{\mu}^F$, the vector of the standard deviations $\vec{\sigma}^F$, and the correlation matrix ρ^F as

$$\vec{\mu}^F = (0.310, 1.55 \cdot 10^{-2}, 1.24 \cdot 10^{-3}, 0.562, 4.03 \cdot 10^{-2}, 4.71 \cdot 10^{-3}), \quad (2.17)$$

$$\vec{\sigma}^F = (0.020, 0.10 \cdot 10^{-2}, 0.10 \cdot 10^{-3}, 0.032, 0.24 \cdot 10^{-2}, 0.37 \cdot 10^{-3}), \quad (2.18)$$

$$\rho^F = \begin{pmatrix} 1.000 & 0.735 & 0.374 & 0.925 & 0.564 & 0.313 \\ 0.735 & 1.000 & 0.867 & 0.927 & 0.863 & 0.246 \\ 0.374 & 0.867 & 1.000 & 0.682 & 0.853 & 0.221 \\ 0.925 & 0.927 & 0.682 & 1.000 & 0.814 & 0.389 \\ 0.564 & 0.863 & 0.853 & 0.814 & 1.000 & 0.647 \\ 0.313 & 0.246 & 0.221 & 0.389 & 0.647 & 1.000 \end{pmatrix}. \quad (2.19)$$

The covariance matrix is then $\Sigma_{ij}^F \equiv \sigma_i^F \sigma_j^F \rho_{ij}^F$.

Note that we obtain an uncertainty on $f_{B\pi}^+(0)$ that is about 20% smaller than the uncertainty given in [10], where similar ranges for the numerical inputs have been used. We expect that further improvement on the precision of $f_{B\pi}^+(0)$ can be achieved if the input

parameters can be further constrained. Inclusion of two-point sum rules for the determination of a_π^2 and a_π^4 , and of experimental measurements of the pion electromagnetic form factors as part of the likelihood are good candidates for such an improvement. Moreover, fits to our LCSR results for the $B \rightarrow \pi$ vector form factor will benefit from the correlation matrix ρ^F , which is computed for the first time.

Our result $f_{B\pi}^+(0) = 0.31 \pm 0.02$ is somewhat larger than the determination in [10], with the value $f_{B\pi}^+(0) = 0.281$ obtained for the central input. Roughly half of the change is due to a slight update of the input parameters, such as the b -quark mass in the $\overline{\text{MS}}$ scheme. We have explicitly checked that our normalization with nominal input parameters as in [10] reproduces their results. The remainder of the change is due to the different statistical treatment, since we quote the mode of the posterior predictive distribution. On the other hand, our result and the one in [10] exhibit a tension with the calculation [14] (and the partial NNLO update [11]). The latter results, obtained in the pole scheme for the b -quark mass, exhibit a smaller central value of $f_{B\pi}^+(0)$. For a detailed discussion on the difference between the respective calculational procedures we refer to [13].

For completeness we also calculate the integral $\Delta\zeta(0, 12\text{GeV}^2)$,

$$\Delta\zeta(0, 12\text{GeV}^2) \equiv \frac{G_F^2}{24\pi^3} \int_0^{12\text{GeV}^2} dq^2 p_\pi^3 |f_{B\pi}^+(q^2)|^2 = (5.25_{-0.54}^{+0.68}) \text{ps}^{-1}, \quad (2.20)$$

where $p_\pi = \sqrt{(m_B^2 + m_\pi^2 - q^2)^2/4m_B^2 - m_\pi^2}$ is the pion's spatial momentum in the B -meson rest frame. The integration range of $\Delta\zeta$ covers the adopted domain of validity for the LCSR. Our $\Delta\zeta$ is compatible with the results of [10], with a relative increase of 14%. This larger central value is consistent with the increase by 8% in the normalization of the central value of the form factor.

3 Extrapolation of the form factor toward large momentum transfer

Having calculated the form factor in the LCSR region, we now turn to an extrapolation toward large momentum transfer q^2 . To this end, we employ a z -series parametrization where we transform the q^2 -variable in the standard way:

$$z(q^2, t_0) = \frac{\sqrt{t_+ - q^2} - \sqrt{t_+ - t_0}}{\sqrt{t_+ - q^2} + \sqrt{t_+ - t_0}}. \quad (3.1)$$

Here and throughout we use $t_\pm \equiv (m_B \pm m_\pi)^2$ and adopt t_0 following [12],

$$t_{0,\text{opt}} = (m_B + m_\pi) \cdot (\sqrt{m_B} - \sqrt{m_\pi})^2 \simeq 20 \text{GeV}^2, \quad (3.2)$$

so that $|z|$ is sufficiently small in the semileptonic region $0 < q^2 < t_-$,

$$|z(q^2, t_{0,\text{opt}})| < 0.280, \quad (3.3)$$

and $z(q^2, t_0)$ is positive in the domain of validity of the LCSR.

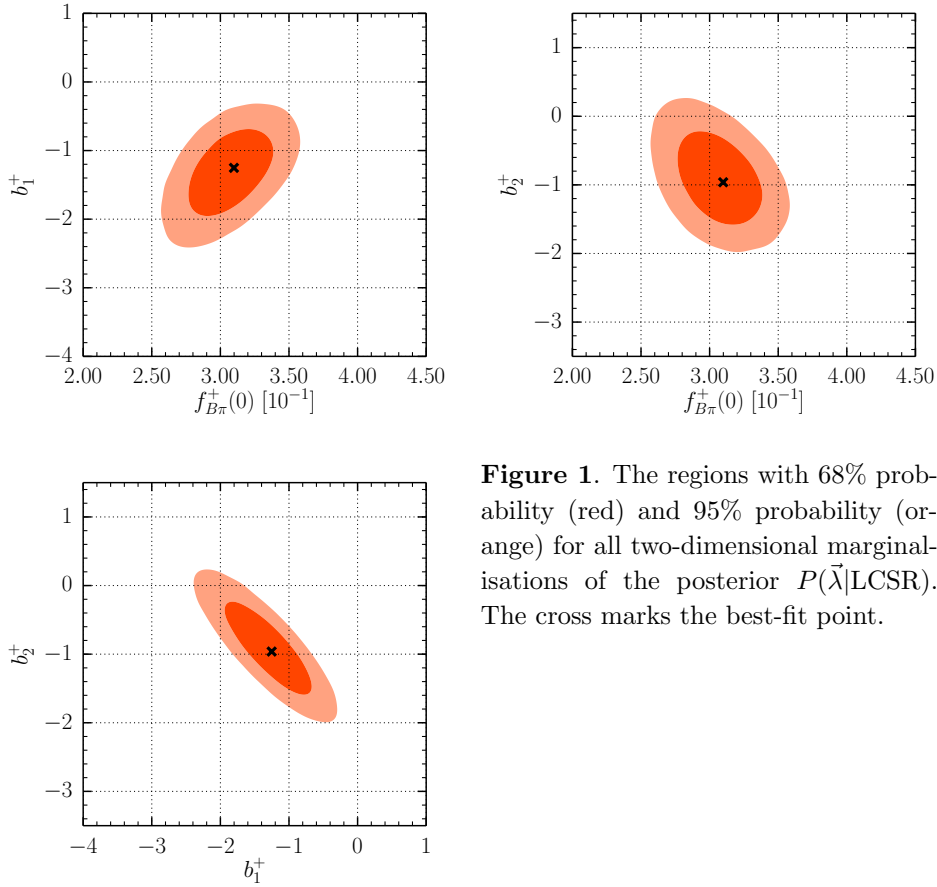


Figure 1. The regions with 68% probability (red) and 95% probability (orange) for all two-dimensional marginalisations of the posterior $P(\vec{\lambda}|\text{LCSR})$. The cross marks the best-fit point.

In what follows, we use the $K = 3$ form of the z -series expansion [12], modified to use the form factor at $q^2 = 0$ as one of the parameters. It is given by the three-parameter expression:

$$f_{B\pi}^+(q^2) = \frac{f_{B\pi}^+(0)}{1 - q^2/m_{B^*}^2} \left\{ 1 + b_1^+ \left[z(q^2, t_0) - z(0, t_0) - \frac{1}{3} \left(z(q^2, t_0)^3 - z(0, t_0)^3 \right) \right] + b_2^+ \left[z(q^2, t_0)^2 - z(0, t_0)^2 + \frac{2}{3} \left(z(q^2, t_0)^3 - z(0, t_0)^3 \right) \right] \right\}. \quad (3.4)$$

The form factor is parametrized in terms of $f_{B\pi}^+(0)$, as well as the two shape parameters b_1^+ and b_2^+ . An analogous but somewhat simpler expression with only one shape parameter was used in previous works [10, 23].

We fit the parametrization eq. (3.4) to our LCSR results, which are incorporated in the likelihood

$$P(\text{LCSR}|\vec{\lambda}) \equiv \mathcal{N}_6(\vec{\mu}^F, \Sigma^F; \vec{F}(\vec{\lambda})), \quad (3.5)$$

with $\vec{\mu}^F$ and Σ^F as determined in section 2; see eqs. (2.17)–(2.19). We choose the prior $P_0(\vec{\lambda})$ as uniform for all three BCL parameters $\vec{\lambda} = (f_{B\pi}^+(0), b_1^+, b_2^+)$, with the respective

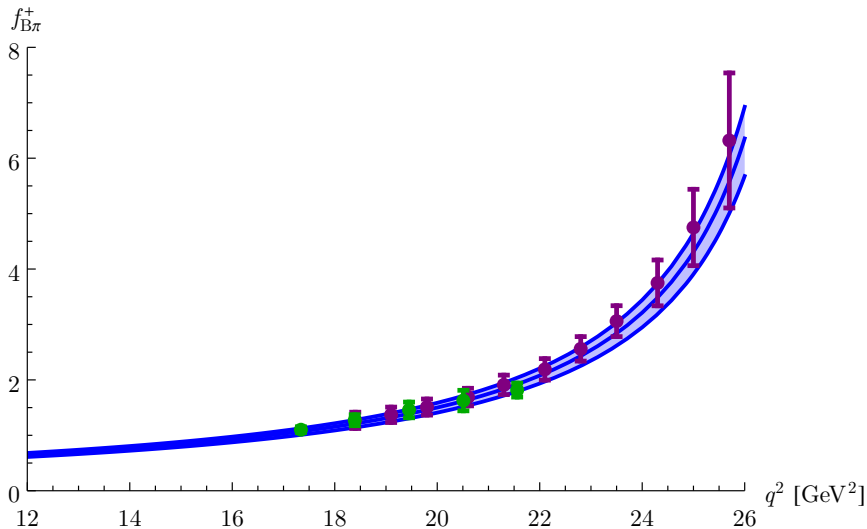


Figure 2. Form factor $f_{B\pi}^+(q^2)$ obtained at $q^2 < 12\text{GeV}^2$ from the statistical analysis of LCSR, fitted to z-series representation and extrapolated to large q^2 . The solid lines correspond to the 68% probability envelope and the best fit curve. The green (magenta) points are HPQCD [7] (Fermilab-MILC [8]) lattice QCD results.

support intervals

$$0 \leq f_{B\pi}^+(0) \leq 1, \quad -10 \leq b_1^+ \leq +10, \quad -10 \leq b_2^+ \leq +10. \quad (3.6)$$

From this follows the posterior distribution $P(\vec{\lambda}|\text{LCSR})$, which turns out to be gaussian to very good approximation. This is evidenced by very small skewness $|\text{Skew}| < 0.2$, and kurtosis $|\text{Kurt}| < 0.2$. We therefore choose to approximate the posterior as

$$P(\vec{\lambda}|\text{LCSR}) \simeq \mathcal{N}_3(\mu^{\text{BCL}}, \Sigma^{\text{BCL}}; \vec{\lambda}), \quad (3.7)$$

where

$$\vec{\mu}^{\text{BCL}} = (0.307, -1.31, -0.904), \quad (3.8)$$

$$\vec{\sigma}^{\text{BCL}} = (0.020, 0.42, 0.444), \quad (3.9)$$

$$\rho^{\text{BCL}} = \begin{pmatrix} 1.000 & 0.503 & -0.391 \\ 0.503 & 1.000 & -0.824 \\ -0.391 & -0.824 & 1.000 \end{pmatrix}, \quad (3.10)$$

and with $\Sigma^{\text{BCL}} \equiv \sigma_i^{\text{BCL}} \sigma_j^{\text{BCL}} \rho_{ij}^{\text{BCL}}$.² For the best-fit point we obtain

$$\vec{\lambda}_{\text{LCSR}}^* \equiv \text{argmax} P(\vec{\lambda}|\text{LCSR}) = (0.310, -1.25, -0.962). \quad (3.11)$$

The goodness of fit is excellent, with $\chi^2 = 1 \cdot 10^{-7}$. For this fit we count our predictions as six observations. Our three fit parameters thus reduce the number of degrees of freedom

²In addition, a data file containing 10^5 weighted variates of the posterior can be obtained from the authors upon request.

q^2	$f_{B\pi}^+(q^2)$	Pull	q^2	$f_{B\pi}^+(q^2)$	Pull
Fermilab-MILC			Fermilab-MILC		
18.4	1.27	+0.39	25.0	4.75	+0.64
19.1	1.37	+0.32	25.7	6.32	+0.61
19.8	1.51	+0.35	26.5	9.04	+0.36
20.6	1.69	+0.31	HPQCD		
21.3	1.91	+0.41	17.34	1.101	+0.58
22.1	2.19	+0.38	18.39	1.273	+0.62
22.8	2.56	+0.58	19.45	1.458	+0.48
23.5	3.06	+0.79	20.51	1.627	+0.04
24.3	3.75	+0.64	21.56	1.816	-0.83

Table 2. The pull values of lattice data points from Fermilab-MILC [8] and HPQCD [7] with respect to our z -series extrapolation of the LCSR results. The extrapolation is obtained from the best-fit point λ^* , see text. The sum of the χ^2 values are 1.72 and 3.67 for HPQCD and Fermilab-MILC, respectively.

down to $N_{\text{d.o.f.}} = 3$. Using the corresponding χ^2 distribution, we estimate a p value of > 0.99 . For completeness, we show the 68% and 95% contours for all two-dimensional marginalisations of the posterior in figure 1.

We compare the extrapolation of our LCSR results of $f_{B\pi}^+$ to large q^2 with lattice data points from the HPQCD [7] and the Fermilab-MILC [8] collaborations in figure 2. There, the filled region corresponds to possible values of the form factor at 68% probability. We also compute the pull values of the best-fit extrapolation with the respective data points in table 2,

$$\text{pull} \equiv \frac{[f_{B\pi}^+(q^2)]_{\text{lattice}} - [f_{B\pi}^+(q^2)]_{\text{extrap.}}}{\sigma_{\text{lattice}}}, \quad (3.12)$$

where σ_{lattice} denotes the uncertainty for the respective lattice point. Without information on the correlation among the lattice results, we cannot compute their goodness of fit with respect to our best-fit-point. However, we do compute the pull values on a point-by-point basis, and find no pull in excess of 0.83σ . We consider this a good agreement between our extrapolation and the lattice results. Furthermore, we observe that, except for one HPQCD lattice point, all lattice points listed in table 2 exhibit positive pull values, which indicates that the lattice results are systematically larger than favoured by our extrapolation. This is of special interest in light of recent preliminary lattice QCD results [31], which are smaller than the published results listed in table 2. The observed trend toward positive pull values could, for instance, be explained by different shapes of the form factors as computed using LCSR and lattice QCD. However, in absence of correlation information for the lattice QCD results, a more detailed comparison of the shapes is not yet possible.

4 Estimation of the strong $B^*B\pi$ coupling

It is well known that the $B \rightarrow \pi$ form factor obeys a rigorous hadronic dispersion relation without subtractions, which reads

$$f_{B\pi}^+(q^2) = \frac{g_{B^*B\pi}f_{B^*}}{2m_{B^*}(1 - q^2/m_{B^*}^2)} + \frac{1}{\pi} \int_{t_+}^{\infty} dt \frac{\text{Im}f_{B\pi}^+(t)}{t - q^2}. \quad (4.1)$$

Here, the residue of the B^* -pole located below threshold t_+ is proportional to the strong $B^*B\pi$ coupling, and to the B^* decay constant that is defined as $\langle 0|\bar{u}\gamma^\mu b|B^*(p, \epsilon_{B^*})\rangle = f_{B^*}m_{B^*}\epsilon_{B^*}^\mu$. For the decay constant we use

$$f_{B^*} = 210 \pm 11 \text{ MeV}, \quad (4.2)$$

which was recently obtained from a 2-point QCD sum rule with NNLO accuracy [24]. It is instructive to compare our above extrapolation to large q^2 with this dispersion relation. First of all, owing to the fact that the B^* pole is embedded in the BCL-ansatz, we can directly estimate the strong coupling. It can be obtained as the residue of the B^* -pole from eq. (3.4):

$$g_{B^*B\pi} = \frac{2m_{B^*}}{f_{B^*}} \lim_{q^2 \rightarrow m_{B^*}^2} \left[(1 - q^2/m_{B^*}^2) f_{B\pi}^+(q^2) \right]. \quad (4.3)$$

We find

$$g_{B^*B\pi} = 30 \pm 5, \quad (4.4)$$

at 68% probability. Note that since this estimate is obtained through an extrapolation slightly beyond the semileptonic region, an additional "systematic" error related to the truncation of z series is expected, according to [12]. The interval eq. (4.4) is in the same ballpark as the first LCSR determination of this hadronic matrix element [19], see also [14, 32]. An update of the LCSR for $g_{B^*B\pi}$ with a better precision than our extrapolation-based result would therefore be useful to anchor the BCL parametrization at large q^2 -values.

Lattice QCD results on the $B^*B\pi$ coupling are usually presented in a form of the effective coupling g_b in the heavy-meson chiral perturbation theory; at leading order the relation is

$$\frac{2m_B}{f_\pi} g_b = g_{B^*B\pi}, \quad (4.5)$$

so that from (4.4) we obtain $g_b = 0.35 \pm 0.06$. This value is compatible with, but smaller than, most lattice QCD results, e.g. $g_b = 0.449 \pm 0.047 \pm 0.019$ [33]. Since our extrapolation (4.4) estimates the strong $B^*B\pi$ coupling in full QCD at finite b quark mass, the issue of inverse heavy-mass corrections is important for this comparison, but remains outside the scope of our present work.

Returning to the dispersion relation (4.1) and substituting the residue of the B^* pole, we are now in a position to estimate the integral on r.h.s. at various q^2 , assessing the cumulative contribution to $f_{B\pi}^+(q^2)$ of radially excited and continuum states with B^* quantum numbers. It is easy to notice that at $q^2 = 0$ this contribution is comparable with the one from B^* -pole but has an opposite sign.

5 Unitarity bounds with inputs from LCSR

The z -parametrization of the form factor $f_{B\pi}^+(q^2)$ obtained from LCSR results has a truncated form depending on the maximal power chosen in the Taylor series at $z = 0$. It is important to test the extrapolations beyond the LCSR region that are based on this parametrization. To this end, we suggest to use the upper and lower bounds on the form factor $f_{B\pi}^+(q^2)$ that are obtained from the unitarity of the correlation function of the b -flavoured vector currents, combined with the input from the LCSR calculation. Since the unitarity bounds are valid in the whole semileptonic region, they are independent of any parametrization of the form factor.

For $B \rightarrow \pi$ form factors the unitarity bounds have been derived in [34], following an earlier work [35]. One starts from the two-point correlation function:

$$\begin{aligned}\Pi_{\mu\nu}(q) &= i \int d^4x e^{iq \cdot x} \langle 0 | T \{ \bar{u} \gamma_\mu b(x), \bar{b} \gamma_\nu u(0) \} | 0 \rangle \\ &= (-g_{\mu\nu} q^2 + q_\mu q_\nu) \tilde{\Pi}_T(q^2) + q_\mu q_\nu \Pi_L(q^2).\end{aligned}\quad (5.1)$$

In what follows, we only need the transverse invariant amplitude $\tilde{\Pi}_T(q^2)$, multiplying it by q^2 to avoid kinematical singularities. It is calculated at $q^2 \ll m_b^2$ using an OPE in terms of the same condensate densities as used in the two-point sum rule eq. (2.7). We update the calculation of eq. (5.1) with respect to the previous analyses of the bounds, adding the NNLO, $O(\alpha_s^2)$ correction to the perturbative part and the NLO, $O(\alpha_s)$ correction to the quark-condensate part. To this end, we use the results of [24] where the same correlation function was employed to obtain the QCD sum rule for the decay constant of the B^* meson. The input parameters needed to calculate (5.1) are the same as for the correlation function of the pseudoscalar b -flavoured currents used for the f_B calculation and are already specified in table 1.

As a further step we match the OPE result to the hadronic dispersion relation and subsequently differentiate both sides of this relation $n + 1$ times with respect to q^2 at $q^2 = \tilde{q}^2 \ll m_b^2$:

$$\chi_T^{(\text{OPE})}(\tilde{q}^2, n) \equiv \frac{1}{(n+1)!} \left(\frac{\partial}{\partial q^2} \right)^{n+1} [q^2 \tilde{\Pi}_T^{(\text{OPE})}(q^2)] \Big|_{q^2=\tilde{q}^2} = \int_{m_{B^*}^2}^{\infty} dt \frac{\rho_T(t)}{(t - \tilde{q}^2)^{n+2}}, \quad (5.2)$$

where $\rho_T(t) \equiv \frac{1}{\pi} \text{Im}[t \tilde{\Pi}_T(t)]$ is the hadronic spectral density. Note that the dispersion integral converges for $n \geq 1$ as follows from QCD asymptotics of the perturbative part of the correlation function. At $n = 1$, eq. (5.2) coincides with the standard double-subtracted dispersion relation used in [34]. According to the unitarity condition, $\rho_T(s)$ contains positive contributions of all possible hadronic states with the B^* quantum numbers. The ground B^* -state contribution to the r.h.s. of differentiated dispersion relation has a form:

$$\chi_T^{(B^*)}(\tilde{q}^2, n) = \frac{f_{B^*}^2 m_{B^*}^2}{(m_{B^*}^2 - \tilde{q}^2)^{n+2}}, \quad (5.3)$$

where for the decay constant f_{B^*} we use the interval eq. (4.2). The hadronic continuum state $|B\pi\rangle$ in P -wave, with the threshold t_+ located slightly above $m_{B^*}^2$, interests us because its contribution to eq. (5.2) contains the integral over the $B \rightarrow \pi$ vector form factor squared:

$$\chi_T^{(B\pi)}(\tilde{q}^2, n) = \int_{t_+}^{\infty} dt k_T(t, \tilde{q}^2, n) |f_{B\pi}^+(t)|^2, \quad (5.4)$$

where the function

$$k_T(s, \tilde{q}^2, n) = \frac{1}{32\pi^2} \frac{[(t-t_+)(t-t_-)]^{3/2}}{t^2(t-\tilde{q}^2)^{n+2}}, \quad (5.5)$$

contains all kinematical factors. In the above, we also take into account the isospin weights of the two (equal in the isospin limit) contributions $\bar{B}^0\pi^-$ and $B^-\pi^0$ with $b\bar{u}$ quantum numbers. A straightforward upper limit for the integrated form factor squared follows then from eq. (5.2):

$$\chi_T^{(B\pi)}(\tilde{q}^2, n) \leq \chi_T^{(\text{OPE})}(\tilde{q}^2, n) - \chi_T^{(B^*)}(\tilde{q}^2, n). \quad (5.6)$$

In [34, 35] and in later analyses $n = 1$, $\tilde{q}^2 = 0$ was chosen in the above. We have carried out a detailed investigation, in which we vary n and take also negative values of \tilde{q}^2 . The resulting bounds do not improve upon such a variation. Hence, in what follows we only consider the simplest case $n = 1$, $\tilde{q}^2 = 0$ and abbreviate:

$$\chi^+ \equiv \chi_T^{(\text{OPE})}(0, 1) - \chi_T^{(B^*)}(0, 1), \quad (5.7)$$

so that

$$\chi_T^{(B\pi)}(0, 1) \leq \chi^+. \quad (5.8)$$

To proceed to a more elaborated bound that also includes the above upper limit, we map the momentum transfer variable $q^2 \rightarrow z(q^2, t_0)$ according to eq. (3.1). As a consequence, the region of integration in eq. (5.4) transforms into the unit circle in the z plane. Note that we are free to choose an arbitrary, convenient value of the parameter t_0 in this transformation; i.e., our choice of t_0 need not be the same as in section 3, eq. (3.2). In terms of the new variable, eq.(5.8) takes the form

$$\int_{|z|=1} \frac{dz}{2\pi iz} |\phi(z, 0, 1) f_{B\pi}^+(t(z, t_0))|^2 \leq \chi^+, \quad (5.9)$$

where $t(z)$ is the inverse of the transformation eq. (3.1). Hereafter we suppress the fixed parameter t_0 in the argument of z -variable for brevity. In the above, $\phi(z, \tilde{q}^2, n)$, given in Appendix, is the outer function, which is analytic and without zeros at $|z| < 1$, and whose modulus on the boundary $|z| = 1$ is related to the kinematical weight function eq. (5.5) and the Jacobian of the transformation eq. (3.1).

Furthermore, one introduces a general definition of the inner product of two functions, integrating the product of $f_1(z)$ and the complex conjugate of $f_2(z)$ on the unit circle:

$$\langle f_2 | f_1 \rangle = \int_{|z|=1} \frac{dz}{2\pi iz} f_2^*(z) f_1(z). \quad (5.10)$$

In terms of this definition eq. (5.9) can be rewritten as

$$\langle \phi f_{B\pi}^+ | \phi f_{B\pi}^+ \rangle \equiv \langle h|h \rangle \leq \chi^+, \quad (5.11)$$

where we denote:

$$h(z) \equiv \phi(z, 0, 1) f_{B\pi}^+(q^2(z)). \quad (5.12)$$

Note that our choice of the outer function contains the Blaschke factor, which effectively removes the B^* pole; see the appendix. As a consequence, the function $h(z)$ is analytic at $|z| < 1$, and real-valued for $z \in (-1, +1)$. Employing the Cauchy theorem with the circle $|z| = 1$ taken as a contour in the complex z -plane, one finds the value of this function at any point $z(q^2)$ of the real z -axis in terms of the inner product:

$$h(z(q^2)) = \langle g|h \rangle, \quad (5.13)$$

where

$$g(z(q^2), z(t)) = \frac{1}{1 - z^*(q^2)z(t)}. \quad (5.14)$$

In the above, we distinguish the z -values on the real axis and on the unit circle by labeling their arguments as q^2 (in the semileptonic region) and t (at $t \geq t_+$), respectively.

In [34], the lattice QCD values of the form factor were employed as an additional input, leading to a substantial improvement of the resulting bounds at large q^2 . Accordingly, we can adopt as an input the values of the form factor as obtained from LCSR at an accessible small and intermediate values of q^2 . More specifically, in our analysis we follow [36], where it was noticed that it is more effective to use as an input the value, first and second derivative of the form factor calculated at one given value q_0^2 ; i.e., $f_{B\pi}^+(q_0^2)$, $f_{B\pi}^{\prime+}(q_0^2)$ and $f_{B\pi}^{\prime\prime+}(q_0^2)$, respectively.³ Hence, we will use the results of the LCSR obtained at $q_0^2 = 10 \text{ GeV}^2$ and presented in section 2. Having at hand these three LCSR inputs and the explicit form of the outer function presented in the appendix, we calculate at $z_0 \equiv z(q_0^2)$ the function eq. (5.12) and its first and second derivative. We abbreviate

$$h(z_0) \equiv h_0, \quad \left. \frac{dh(z)}{dz} \right|_{z=z_0} \equiv h_1, \quad \left. \frac{1}{2} \frac{d^2h(z)}{dz^2} \right|_{z=z_0} \equiv h_2. \quad (5.15)$$

Simultaneously, we adopt $t_0 = q_0^2$ so that $z_0 = 0$.

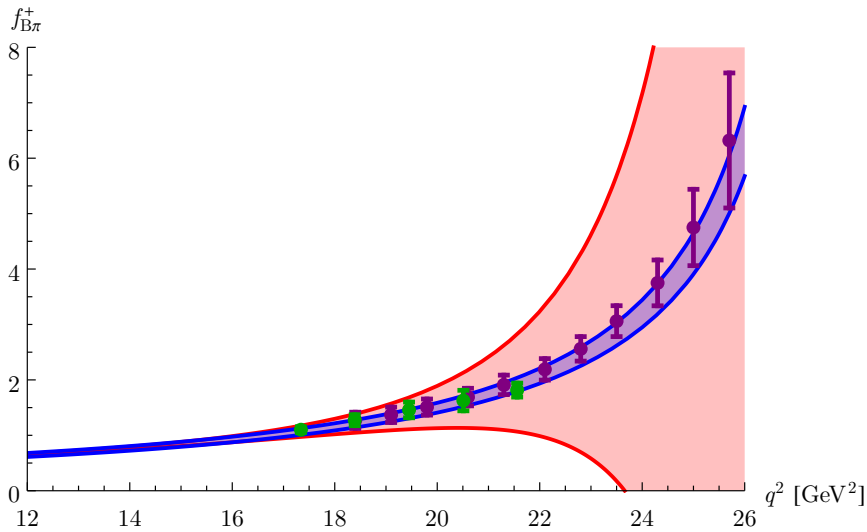
For the sake of generality we prefer to keep $z_0 \neq 0$ and consider three points on the real z axis: z_0 , $z_0 + \epsilon$ and $z_0 - \epsilon$ where ϵ is an arbitrarily small interval, so that

$$h(z_0 \pm \epsilon) = h_0 \pm h_1 \epsilon + h_2 \epsilon^2 + O(\epsilon^3). \quad (5.16)$$

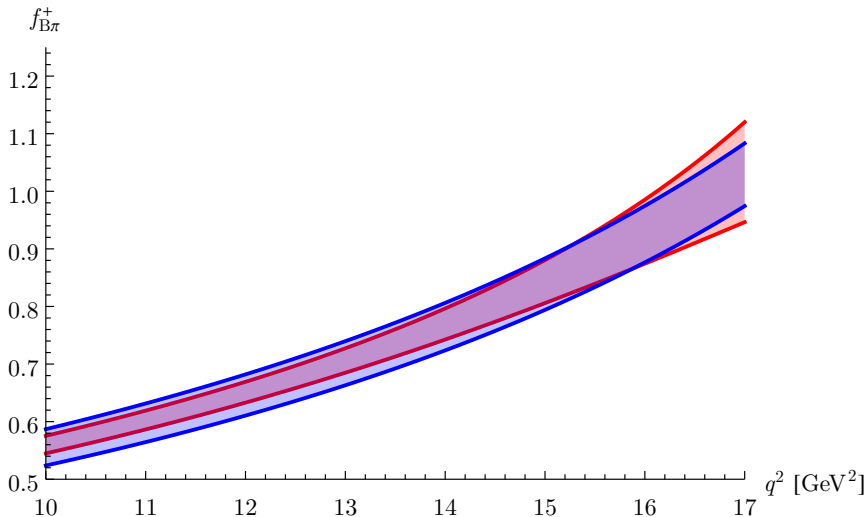
The values of $h(z_0)$ and $h(z_0 \pm \epsilon)$ (the latter with $O(\epsilon^2)$ accuracy) can be transformed to the form of inner products similar to eq. (5.13):

$$h(z_0) = \langle g_0|h \rangle, \quad h(z_0 + \epsilon) = \langle g_+|h \rangle, \quad h(z_0 - \epsilon) = \langle g_-|h \rangle, \quad (5.17)$$

³A different approach to include the values of the form factors and their higher derivatives is based [37] on Lagrange multipliers and analytic interpolation theory, and leads to similar results.



(a)



(b)

Figure 3. Unitarity bounds (red shaded area) based on the LCSR input at $q^2 = 10 \text{ GeV}^2$ in comparison with the lattice QCD results (green points: HPQCD [7], magenta points: Fermilab-MILC [8]) and our extrapolation based on the BCL parametrization (blue shaded area).

where $g_0 \equiv g(z_0, z(t))$ and $g_{\pm} \equiv g(z_0 \pm \epsilon, z(t))$.

The next step is to form a 5×5 matrix \mathcal{M} that is obtained by combining all diagonal and nondiagonal inner products of the above three functions, together with the functions $g(z(q^2), z(t))$ and $h(z(q^2))$. The latter depends on the form factor $f_{B\pi}^+(q^2)$ at a certain value q^2 within the semileptonic region.

The explicit form of this matrix, given in the appendix, is obtained after applying Cauchy's theorem for each inner product, except for the first diagonal matrix element $\langle h|h \rangle$, and by employing the approximation eq. (5.16). We then use the positivity of all

matrix elements of \mathcal{M} from which the condition $\det \mathcal{M} \geq 0$ follows.⁴ The latter can be rewritten in the form of quadratic inequality with respect to $h(z)$:

$$\langle h|h \rangle d + a h(z)^2 + b h(z) + c \geq 0. \quad (5.18)$$

The coefficients a, b, c, d are functions of ϵ and the input parameters $h_{0,1,2}$. Inspection of these coefficients shows that all of them are proportional to ϵ^6 and the coefficient d is positive. Hence, one can replace the diagonal inner product $\langle h|h \rangle$ in the above by the upper limit eq. (5.11) and simultaneously rescale the coefficients. The resulting inequality is valid at all (sufficiently small) ϵ , and a smooth limit $\epsilon \rightarrow 0$ is applicable. The two roots of the quadratic inequality yield the upper and lower limits for the function $h(z)$. Application of (5.12) allows us to convert the latter into upper and lower bounds on the form factor $f_{B\pi}^+$. The result is especially simple at our choice $q_0^2 = t_0$ and $z_0 = 0$:

$$\left[f_{B\pi}^+(q^2(z)) \right]_{\text{low}}^{\text{up}} = \frac{1}{\phi(z, 0, 1)} \left(h_0 + h_1 z + h_2 z^2 \pm \sqrt{\frac{z^6}{1-z^2} (\chi^+ - h_0^2 - h_1^2 - h_2^2)} \right). \quad (5.19)$$

For a numerical computation of the bounds we require the form factor and its first and second derivative at $q^2 = q_0^2 = 10 \text{ GeV}^2$:

$$\vec{F}_{10} \equiv (f_{B\pi}^+(10 \text{ GeV}^2), f_{B\pi}^{+'}(10 \text{ GeV}^2), f_{B\pi}^{+''}(10 \text{ GeV}^2)).$$

Through marginalisation of $P(\vec{F}|m_B)$ (see eq. (2.15)), we obtain the required posterior predictive distribution $P(\vec{F}_{10}|m_B)$, which we then use to compute the predictive distributions for the bounds as functions of q^2 . For simplicity, the value of χ^+ is computed only for the central input from table 1, after having checked that a variation of the differentiated two-point correlation function at $q^2 = 0$ produces a negligible impact on the bounds. We obtain samples of the predictive distributions for both the upper and the lower bounds, and consequently their respective cumulative distributions. We proceed to compute the values $f_{B\pi, \text{up(low)}}^+(q^2)$ at 68% (1 – 68%) cumulative probability, which are displayed as the red-shaded area in figure 3, together with the lattice QCD results and our extrapolations based on the BCL parametrization. We observe that the bounds are obeyed by the central value of our extrapolation. For $q^2 < 16 \text{ GeV}^2$, the bounds are somewhat more constraining than the 68%-probability envelope, see figure 3(b). This is not unexpected due to the fact that the bounds and the extrapolation follow from different statistical analyses. Interestingly enough, the bounds are constraining the lattice results quite critically at $q^2 < 20 \text{ GeV}^2$.

6 Determination of $|V_{ub}|$ from $\bar{B}^0 \rightarrow \pi^+ \ell^- \bar{\nu}$ decays

As the final step of this work we apply our results from section 2 to a determination of $|V_{ub}|$ from $B \rightarrow \pi \ell \nu$ decays. For this, we carry out a combined Bayesian fit of both $|V_{ub}|$ and the BCL parametrization eq. (3.4) to the LCSR results and corresponding experimental results by the BaBar and Belle collaborations [2–5]. To this end, we extend EOS [30]

⁴The simplest mathematical construction of this type, without any inputs, leads to a 2×2 matrix, see e.g., [34].

Data set	pull [σ]			χ^2	p value	$\log(Z)$
	LCSR	BaBar	Belle			
D_{2010}	0.71	1.78	1.38	5.58	0.98	166.02
D_{2013}	0.28	3.07	2.20	14.34	0.42	155.48

Table 3. Goodness-of-fit quantities for both the “2010” and the “2013” data sets, assuming $N_{\text{d.o.f}} = 14$ degrees of freedom. All pulls follow from a (multivariate) gaussian distribution. Here, $Z \equiv \int d\vec{x} P(\vec{x}|D)P_0(\vec{x})$ denotes the evidence.

by implementing the relevant branching ratio for $\bar{B}^0 \rightarrow \pi^+ \ell \bar{\nu}_\ell$ decays, as well as the experimental likelihoods. All estimation of probability regions follow from the algorithm as developed in [38], which is implemented within EOS.

Let $\vec{x} = (|V_{ub}|, f_{B\pi}^+(0), b_1^+, b_2^+)$ denote the fit parameters. We construct the prior $P_0(\vec{x})$ using uniform distributions with the support

$$\begin{aligned} 1 \leq 10^3 |V_{ub}| \leq 6, \quad -10 \leq b_1^+ \leq +10, \\ 0 \leq f_{B\pi}^+(0) \leq 1, \quad -10 \leq b_2^+ \leq +10. \end{aligned} \quad (6.1)$$

We perform two individual fits to the data sets “2010” and “2013”,

$$\begin{aligned} D_{2010} &\equiv \text{LCSR} \oplus \text{BaBar}_{2010} \oplus \text{Belle}_{2010}, \quad [2, 3] \\ D_{2013} &\equiv \text{LCSR} \oplus \text{BaBar}_{2012} \oplus \text{Belle}_{2013}. \quad [4, 5] \end{aligned} \quad (6.2)$$

Their respective likelihoods are formed as product of $P(\text{LCSR}|\vec{x})$ (compare eq. (3.5)) with the individual experimental likelihoods. We use exclusively the experimental results on the decay $\bar{B}^0 \rightarrow \pi^+ \ell^- \bar{\nu}_\ell$, with kinematical cuts $0 \leq q^2 \leq 12 \text{ GeV}^2$. All experiments [2–5] provide their results as mean values $\vec{\mu}^E$ for six q^2 bins of width 2 GeV^2 , and include sufficient information to construct the covariance matrices Σ^E . Thus, we use $P(E|\vec{x}) = \mathcal{N}_6(\vec{\mu}^E, \Sigma^E|\vec{x})$, for $E = \text{BaBar}_{2010}, \text{Belle}_{2010}, \text{BaBar}_{2012}$ and Belle_{2013} , respectively.

We obtain posterior distributions from our prior and the likelihoods. From the posteriors follow two best-fit points for the individual experimental data sets,

$$\begin{aligned} \vec{x}_{2010}^* &= \text{argmax} P(\vec{x}|D_{2010}) = (3.44 \cdot 10^{-3}, 0.281, -2.14, -0.364), \\ \vec{x}_{2013}^* &= \text{argmax} P(\vec{x}|D_{2013}) = (3.33 \cdot 10^{-3}, 0.288, -1.94, -0.465), \end{aligned} \quad (6.3)$$

When compared to the best-fit point λ_{LCSR}^* (see eq. (3.11)), the above two points exhibit a marked negative shift in the parameter b_1^+ of $-0.89 \simeq 74\%$ and $-0.69 \simeq 58\%$ for the 2010 and 2013 data sets, respectively. In order to calculate the goodness of fit, we assume $N_{\text{d.o.f.}} = 14$ degrees of freedom, which follows from 18 observations (6 theoretical inputs and 12 experimental observations), reduced by $\dim \vec{x} = 4$ fit parameters. The p values follow from a χ^2 -distribution with $N_{\text{d.o.f.}}$ degrees of freedom for the pull values at the respective best-fit point.

We find a good fit, with p values 0.98 and 0.42 for the “2010” and “2013” data sets, respectively. We proceed to calculate the Bayes factor for both data sets, and obtain

$$\frac{P(D_{2010})}{P(D_{2013})} \equiv \frac{\int d\vec{x} P(D_{2010}|\vec{x})P_0(\vec{x})}{\int d\vec{x} P(D_{2013}|\vec{x})P_0(\vec{x})} = 3.8 \cdot 10^4. \quad (6.4)$$

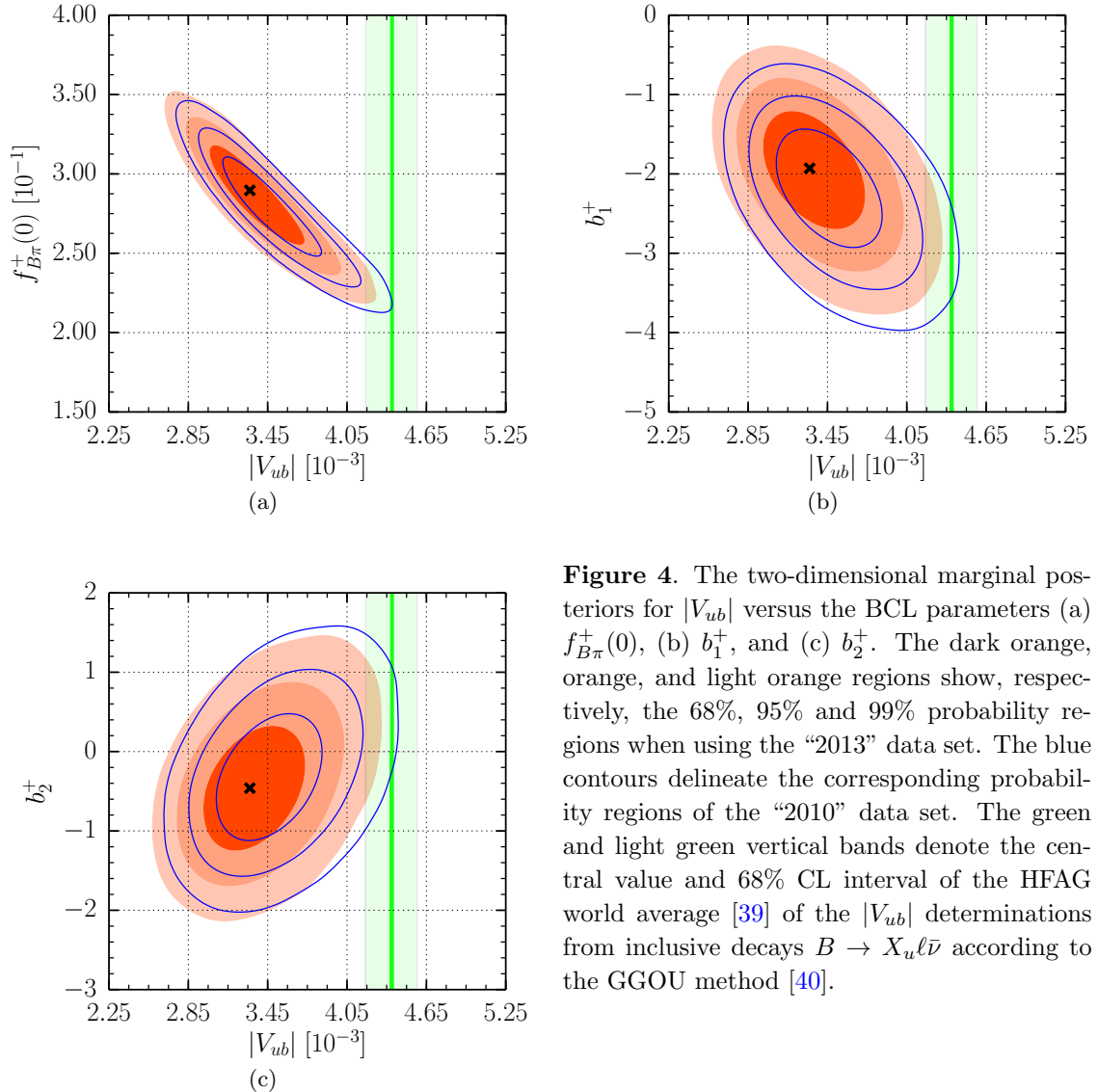


Figure 4. The two-dimensional marginal posteriors for $|V_{ub}|$ versus the BCL parameters (a) $f_{B\pi}^+(0)$, (b) b_1^+ , and (c) b_2^+ . The dark orange, orange, and light orange regions show, respectively, the 68%, 95% and 99% probability regions when using the “2013” data set. The blue contours delineate the corresponding probability regions of the “2010” data set. The green and light green vertical bands denote the central value and 68% CL interval of the HFAG world average [39] of the $|V_{ub}|$ determinations from inclusive decays $B \rightarrow X_u \ell \bar{\nu}$ according to the GGOU method [40].

The hypothesis “LCSR results are in agreement with 2010 data” is therefore decisively favoured over the hypothesis “LCSR results are in agreement with 2013 data”. The remainder of the goodness-of-fit values for both data sets is displayed in table 3.

We show the 68%, 95% and 99% probability regions of those two-dimensional marginal distribution that involve $|V_{ub}|$ for both data sets in figure 4. There we also compare our determination of $|V_{ub}|$ from $B^0 \rightarrow \pi^+ \ell \bar{\nu}_\ell$ with the HFAG world average of the inclusive determination according to GGOU [40],

$$|V_{ub}|^{\text{HFAG,GGOU}} = (4.39 \pm 0.15^{+0.12}_{-0.14}) \cdot 10^{-3}. \quad (6.5)$$

We find that the “2010” data set is compatible with the inclusive determination at the 3σ level. However, the “2013” data set moves even further away from the inclusive values.

Through integration over all BCL parameters we obtain the one-dimensional marginal posteriors $P(|V_{ub}| | D_{2010})$ and $P(|V_{ub}| | D_{2013})$.⁵ Their respective 68% probability intervals read

$$\begin{aligned} |V_{ub}|^{2010} &= (3.43_{-0.23}^{+0.27}) \cdot 10^{-3}, \\ |V_{ub}|^{2013} &= (3.32_{-0.22}^{+0.26}) \cdot 10^{-3}. \end{aligned} \tag{6.6}$$

Both intervals are compatible with each other at a level of less than 1σ .

7 Conclusion

We have carried out the first Bayesian analysis of the $B \rightarrow \pi$ vector form factor within the framework of LCSR in QCD. For this, it was instrumental to construct a likelihood that relates the sum rule to the experimentally measured B -meson mass. As a consequence, our analysis yields correlated constraints on the input parameter space. One of our main results are predictions for the form factor $f_{B\pi}^+(q^2)$ and its derivatives at two separate values of momentum transfer $q^2 = 0$ and 10 GeV^2 , well within the window of applicability of the LCSR. A comprehensive "diagnostics" of the obtained probability distributions for each input parameter is described above.

Based on these results, we obtain a joint posterior-predictive probability distribution for the parameters of the z -series representation. This distribution is urgently needed for the precise extrapolation of $f_{B\pi}^+(q^2)$ toward large q^2 , beyond the LCSR region. Interestingly, we find theoretical uncertainties that are about 20% smaller than those obtained in previous analyses, where only naive estimates — based on individual variations of each input parameter — had been carried out. Especially encouraging is a reasonably small dependence on the combined renormalization/factorization scale, which was separately investigated by varying the combined scale in the same interval as in [10]. All these findings prompt the conclusion that a simultaneous "scanning" of the input parameter space within a Bayesian analysis is probably the only revealing way to assess the realistic uncertainties of a non-lattice QCD-method such as LCSR. Our analysis supports the use of the B -meson mass to constrain the effective threshold interval in the quark-hadron duality approximation.

A word of caution should be added to the above comments, reminding that the accuracy estimated in this paper concerns a certain *approximation* of LCSR, with a truncated OPE and the quark-hadron duality ansatz applied to the correlation function and to the rigorous hadronic dispersion relation. A further improvement of LCSRs is desirable, but demands several technically challenging computations: the complete NNLO corrections to twist 2 and 3 terms; the nonasymptotic corrections to the twist-3 NLO part; and an assessment of twist-5 and 6 terms. On the side of the input parameters, it is desirable to improve our knowledge of the pion DAs. Important constraints on their parameters arise from other LCSRs, such as the ones for the pion electromagnetic form factor and the $\gamma\gamma^* \rightarrow \pi$ form factor. In fact, even more information on the correlations between the various input parameters could be obtained from a global analysis; e.g., by incorporating measurements of the aforementioned form factors into the likelihood.

⁵Variates of either posterior distribution can be obtained from the authors upon request.

Turning to the comparison with other theoretical predictions of the $B \rightarrow \pi$ form factor, we notice that our results at low q^2 are consistent with the outcome of the previous analyses of LCSR, if one adopts the simplified uncertainty estimates in these analyses. Furthermore, our extrapolation to large q^2 is in a very good agreement with the published lattice QCD results.

As a byproduct of our analysis, we can predict the strong $B^*B\pi$ coupling. Our result is in the ballpark of earlier direct LCSR calculations based on double dispersion relations with simple duality ansatz and obtained from a less accurate correlation function. It is therefore important to update the latter calculation and include it in one statistical pool with the $B \rightarrow \pi$ form factor.

The second main result of this paper is the implementation of the model-independent bounds for the form factor, which allow one to confirm the reliability of the extrapolation that is based on truncated z -series. We studied different versions of these bounds and found that the ones which include form factor and its first and second derivative (all at one value of q^2) are the most confining and useful ones. We obtain an upper/lower bound at $q^2 = 20 \text{ GeV}^2$ that is only about $\pm 25\%$ larger/smaller than the average value of the extrapolated form factor. Our findings will be important for the comparison with the respective lattice QCD results, which can currently be calculated at $q^2 \gtrsim 17 \text{ GeV}^2$.

The third main result of this paper is the determination of $|V_{ub}|$ from available experimental data within the region of LCSR. We find that the two sets of experimental analyses are very compatible with the LCSR predictions for the vector form factor. However, based on a Bayesian model comparison, we also find that 2010 data set is in decisively better agreement with the theory predictions than the 2013 data set.

Note that given the approximation of LCSR, the theoretical uncertainty in $|V_{ub}|$ obtained from our analysis is comparable to the one from the most accurate determinations of this CKM parameter in the inclusive $b \rightarrow u$ transitions. We find that our results exhibit a tension with respect to the GGOU determination beyond the level of 99% probability.

Concluding, we foresee an immediate extension of this work to other exclusive $b \rightarrow s$ and $b \rightarrow u$ transitions, comprehensively updating the LCSRs for the $B \rightarrow K$ and $B_s \rightarrow K$ form factors and applying the statistical analysis.

Acknowledgments

D.v.D. would like to thank Frederik Beaujean for helpful discussions. I.S.I. would like to thank Irinel Caprini for useful discussions. This work is supported in parts by the Bundesministerium für Bildung und Forschung (BMBF), and by the Deutsche Forschungsgemeinschaft (DFG), Research Unit FOR 1873 (“Quark Flavour Physics and Effective Field Theories”), Contract No.KH 205/2-1.

A Formulae relevant for the unitarity bounds

1. The expression for the outer function at $\tilde{q}^2 \neq 0$ and $n+1$ differentiations is obtained after transformation of the variable $t \rightarrow z(t, t_0)$ in the kinematical factor $k_T(t, \tilde{q}^2, n)$ entering

the integral (5.4) including also the Jacobian of this transformation:

$$|\phi(z, \tilde{q}^2, n)|^2 \sim k_T(t(z), \tilde{q}^2, n) \frac{dt(z, t_0)}{dz}, \quad (\text{A.1})$$

To obtain a function $\phi(z, \tilde{q}^2, n)$ with desired analytical properties (no poles and/or zeros inside the unit disc) one has to multiply the above expression by unimodular functions that are equal 1 on the unit circle, hence do not change the value of the integral. We skip this part of the derivation for brevity. In addition, in order to eliminate the B^* pole located on the real axis of z plane, the outer function is also multiplied by the (unimodular) Blaschke factor [12, 34],

$$B(z, t_0) = \frac{z - z(m_{B^*}^2, t_0)}{1 - z z(m_{B^*}^2, t_0)}. \quad (\text{A.2})$$

As a result, the outer function at $\tilde{q}^2 \neq 0$ and general number of differentiations n is:

$$\begin{aligned} \phi(z, \tilde{q}^2, n) &= \frac{B(z, t_0)}{\sqrt{32\pi}} \left(\sqrt{t_+ - t(z, t_0)} + \sqrt{t_+ - t_0} \right) \\ &\times \frac{(t_+ - t(z, t_0))}{(t_+ - t_0)^{1/4}} \frac{(\sqrt{t_+ - t_-} + \sqrt{t_+ - t(z, t_0)})^{3/2}}{(\sqrt{t_+} + \sqrt{t_+ - t(z, t_0)})^2 (\sqrt{t_+ + \tilde{q}^2} + \sqrt{t_+ - t(z, t_0)})^{n+2}} \end{aligned} \quad (\text{A.3})$$

At $n = 1$ and $\tilde{q}^2 = 0$ it coincides with the expression given in [12].

2. The 5×5 matrix used for the derivation of the bounds as described in the text has the following expression

$$\mathcal{M} = \begin{pmatrix} \langle h|h \rangle & h_0 & h_0 + h_1\epsilon + h_2\epsilon^2 & h_0 - h_1\epsilon + h_2\epsilon^2 & h(z) \\ h_0 & \frac{1}{1-z_0^2} & \frac{1}{1-z_0(z_0+\epsilon)} & \frac{1}{1-z_0(z_0-\epsilon)} & \frac{1}{1-zz_0} \\ h_0 + h_1\epsilon + h_2\epsilon^2 & \frac{1}{1-z_0(z_0+\epsilon)} & \frac{1}{1-(z_0+\epsilon)^2} & \frac{1}{1-(z_0+\epsilon)(z_0-\epsilon)} & \frac{1}{1-z(z_0+\epsilon)} \\ h_0 - h_1\epsilon + h_2\epsilon^2 & \frac{1}{1-z_0(z_0-\epsilon)} & \frac{1}{1-(z_0+\epsilon)(z_0-\epsilon)} & \frac{1}{1-(z_0-\epsilon)^2} & \frac{1}{1-z(z_0-\epsilon)} \\ h(z) & \frac{1}{1-zz_0} & \frac{1}{1-z(z_0+\epsilon)} & \frac{1}{1-z(z_0-\epsilon)} & \frac{1}{1-z^2} \end{pmatrix} \quad (\text{A.4})$$

where $h_{0,1,2}$ are the shorthand notations introduced in eq. (5.15).

References

- [1] **BaBar** Collaboration, P. del Amo Sanchez et al., *Study of $B \rightarrow \pi \ell \nu$ and $B \rightarrow \rho \ell \nu$ Decays and Determination of $|V_{ub}|$* , *Phys.Rev.* **D83** (2011) 032007, [[arXiv:1005.3288](#)].
- [2] **BaBar** Collaboration, P. del Amo Sanchez et al., *Measurement of the $B^0 \rightarrow \pi^{\ell} \ell^+ \nu$ and $B^+ \rightarrow \eta^{(\prime)} \ell^+ \nu$ Branching Fractions, the $B^0 \rightarrow \pi^- \ell^+ \nu$ and $B^+ \rightarrow \eta \ell^+ \nu$ Form-Factor Shapes, and Determination of $|V_{ub}|$* , *Phys.Rev.* **D83** (2011) 052011, [[arXiv:1010.0987](#)].
- [3] **BELLE** Collaboration, H. Ha et al., *Measurement of the decay $B^0 \rightarrow \pi^- \ell^+ \nu$ and determination of $|V_{ub}|$* , *Phys.Rev.* **D83** (2011) 071101, [[arXiv:1012.0090](#)].

- [4] **BaBar** Collaboration, J. Lees et al., *Branching fraction and form-factor shape measurements of exclusive charmless semileptonic B decays, and determination of $|V_{ub}|$* , *Phys.Rev.* **D86** (2012) 092004, [[arXiv:1208.1253](#)].
- [5] **BELLE** Collaboration, A. Sibidanov et al., *Study of Exclusive $B \rightarrow X_u \ell \nu$ Decays and Extraction of $|V_{ub}|$ using Full Reconstruction Tagging at the Belle Experiment*, *Phys.Rev.* **D88** (2013), no. 3 032005, [[arXiv:1306.2781](#)].
- [6] **Particle Data Group** Collaboration, J. Beringer et al., *Review of Particle Physics (RPP)*, *Phys.Rev.* **D86** (2012) 010001.
- [7] E. Dalgic, A. Gray, M. Wingate, C. T. Davies, G. P. Lepage, et al., *B meson semileptonic form-factors from unquenched lattice QCD*, *Phys.Rev.* **D73** (2006) 074502, [[hep-lat/0601021](#)].
- [8] J. A. Bailey, C. Bernard, C. E. DeTar, M. Di Pierro, A. El-Khadra, et al., *The $B \rightarrow \pi \ell \nu$ semileptonic form factor from three-flavor lattice QCD: A Model-independent determination of $|V_{ub}|$* , *Phys.Rev.* **D79** (2009) 054507, [[arXiv:0811.3640](#)].
- [9] **QCDSF** Collaboration, A. Al-Haydari et al., *Semileptonic form factors $D \rightarrow \pi, K$ and $B \rightarrow \pi, K$ from a fine lattice*, *Eur.Phys.J.* **A43** (2010) 107–120, [[arXiv:0903.1664](#)].
- [10] A. Khodjamirian, T. Mannel, N. Offen, and Y.-M. Wang, *$B \rightarrow \pi \ell \nu_l$ Width and $|V_{ub}|$ from QCD Light-Cone Sum Rules*, *Phys.Rev.* **D83** (2011) 094031, [[arXiv:1103.2655](#)].
- [11] A. Bharucha, *Two-loop Corrections to the $B \rightarrow \pi$ Form Factor from QCD Sum Rules on the Light-Cone and $|V_{ub}|$* , *JHEP* **1205** (2012) 092, [[arXiv:1203.1359](#)].
- [12] C. Bourrely, I. Caprini, and L. Lellouch, *Model-independent description of $B \rightarrow \pi \ell \bar{\nu}$ decays and a determination of $|V_{ub}|$* , *Phys.Rev.* **D79** (2009) 013008, [[arXiv:0807.2722](#)].
- [13] G. Duplancic, A. Khodjamirian, T. Mannel, B. Melic, and N. Offen, *Light-cone sum rules for $B \rightarrow \pi$ form factors revisited*, *JHEP* **0804** (2008) 014, [[arXiv:0801.1796](#)].
- [14] P. Ball and R. Zwicky, *New results on $B \rightarrow \pi, K, \eta$ decay formfactors from light-cone sum rules*, *Phys.Rev.* **D71** (2005) 014015, [[hep-ph/0406232](#)].
- [15] I. Balitsky, V. M. Braun, and A. Kolesnichenko, *$\Sigma^+ \rightarrow P \gamma$ Decay in QCD*, *Sov.J.Nucl.Phys.* **44** (1986) 1028.
- [16] V. M. Braun and I. Filyanov, *QCD Sum Rules in Exclusive Kinematics and Pion Wave Function*, *Z.Phys.* **C44** (1989) 157.
- [17] V. Chernyak and I. Zhitnitsky, *B meson exclusive decays into baryons*, *Nucl.Phys.* **B345** (1990) 137–172.
- [18] V. Belyaev, A. Khodjamirian, and R. Rückl, *QCD calculation of the $B \rightarrow \pi, K$ form-factors*, *Z.Phys.* **C60** (1993) 349–356, [[hep-ph/9305348](#)].
- [19] V. Belyaev, V. M. Braun, A. Khodjamirian, and R. Rückl, *$D^* D \pi$ and $B^* B \pi$ couplings in QCD*, *Phys.Rev.* **D51** (1995) 6177–6195, [[hep-ph/9410280](#)].
- [20] A. Khodjamirian, R. Rückl, S. Weinzierl, and O. I. Yakovlev, *Perturbative QCD correction to the $B \rightarrow \pi$ transition form-factor*, *Phys.Lett.* **B410** (1997) 275–284, [[hep-ph/9706303](#)].
- [21] E. Bagan, P. Ball, and V. M. Braun, *Radiative corrections to the decay $B \rightarrow \pi \ell \nu$ and the heavy quark limit*, *Phys.Lett.* **B417** (1998) 154–162, [[hep-ph/9709243](#)].
- [22] P. Ball, V. Braun, and A. Lenz, *Higher-twist distribution amplitudes of the K meson in QCD*, *JHEP* **0605** (2006) 004, [[hep-ph/0603063](#)].

- [23] A. Khodjamirian, C. Klein, T. Mannel, and N. Offen, *Semileptonic charm decays $D \rightarrow \pi \ell \nu(\ell)$ and $D \rightarrow K \ell \nu(\ell)$ from QCD Light-Cone Sum Rules*, *Phys.Rev.* **D80** (2009) 114005, [[arXiv:0907.2842](#)].
- [24] P. Gelhausen, A. Khodjamirian, A. A. Pivovarov, and D. Rosenthal, *Decay constants of heavy-light vector mesons from QCD sum rules*, *Phys.Rev.* **D88** (2013), no. 1 014015, [[arXiv:1305.5432](#)].
- [25] H. Leutwyler, *The Ratios of the light quark masses*, *Phys.Lett.* **B378** (1996) 313–318, [[hep-ph/9602366](#)].
- [26] B. Ioffe, *Condensates in quantum chromodynamics*, *Phys.Atom.Nucl.* **66** (2003) 30–43, [[hep-ph/0207191](#)].
- [27] S. Agaev, V. Braun, N. Offen, and F. Porkert, *Light Cone Sum Rules for the $\pi^0 - \gamma^* - \gamma$ Form Factor Revisited*, *Phys.Rev.* **D83** (2011) 054020, [[arXiv:1012.4671](#)].
- [28] S. Agaev, V. Braun, N. Offen, and F. Porkert, *BELLE Data on the $\pi^0 \gamma^* \gamma$ Form Factor: A Game Changer?*, *Phys.Rev.* **D86** (2012) 077504, [[arXiv:1206.3968](#)].
- [29] A. Gelman, J. Carlin, H. Stern, D. Dunson, A. Vehtari, and D. Rubin, *Bayesian Data Analysis*. Chapman & Hall/CRC Texts in Statistical Science (Book 106). Chapman and Hall/CRC, 3rd ed., 2013.
- [30] D. van Dyk et al., “EOS: A HEP Program for Flavor Observables.” The version used for this publication is available from <http://project.het.physik.tu-dortmund.de/source/eos/tag/btopi-ff>.
- [31] C. Bouchard, “ $B \rightarrow \pi \ell \nu$ and $B_s \rightarrow K \ell \nu$ from FNAL/HPQCD.” Talk given at “The 8th International Workshop on the CKM Unitarity Triangle”, <http://indico.cern.ch/event/253826/session/5/contribution/57>.
- [32] A. Khodjamirian, R. Rückl, S. Weinzierl, and O. I. Yakovlev, *Perturbative QCD correction to the light cone sum rule for the $B^* B \pi$ and $D^* D \pi$ couplings*, *Phys.Lett.* **B457** (1999) 245–252, [[hep-ph/9903421](#)].
- [33] W. Detmold, C. D. Lin, and S. Meinel, *Calculation of the heavy-hadron axial couplings g_1 , g_2 , and g_3 using lattice QCD*, *Phys.Rev.* **D85** (2012) 114508, [[arXiv:1203.3378](#)].
- [34] L. Lellouch, *Lattice constrained unitarity bounds for $\bar{B}^0 \rightarrow \pi^+ \ell^- \bar{\nu}_\ell$ decays*, *Nucl.Phys.* **B479** (1996) 353–391, [[hep-ph/9509358](#)].
- [35] C. Bourrely, B. Machet, and E. de Rafael, *Semileptonic Decays of Pseudoscalar Particles ($M \rightarrow M' \ell \nu_\ell$) and Short Distance Behavior of Quantum Chromodynamics*, *Nucl.Phys.* **B189** (1981) 157.
- [36] T. Mannel and B. Postler, *Improved unitarity bounds for $\bar{B}^0 \rightarrow \pi^+ \ell \bar{\nu}_\ell(\bar{\ell})$ decays*, *Nucl.Phys.* **B535** (1998) 372–386, [[hep-ph/9805425](#)].
- [37] G. Abbas, B. Ananthanarayan, I. Caprini, I. Sentitemsu Imsong, and S. Ramanan, *Theory of unitarity bounds and low energy form factors*, *Eur.Phys.J.* **A45** (2010) 389–399, [[arXiv:1004.4257](#)].
- [38] F. Beaujean, *A Bayesian analysis of rare B decays with advanced Monte Carlo methods*. PhD thesis, Fakultät für Physik, Technische Universität München, 2012.
- [39] **Heavy Flavor Averaging Group** Collaboration, Y. Amhis et al., *Averages of B-Hadron*,

C-Hadron, and tau-lepton properties as of early 2012, [arXiv:1207.1158](https://arxiv.org/abs/1207.1158). We use the PDG 2013 update from the online version at <http://www.slac.stanford.edu/xorg/hfag>.

- [40] P. Gambino, P. Giordano, G. Ossola, and N. Uraltsev, *Inclusive semileptonic B decays and the determination of $|V_{ub}|$* , *JHEP* **0710** (2007) 058, [[arXiv:0707.2493](https://arxiv.org/abs/0707.2493)].